EEET ECOLOGICAL ENGINEERING & ENVIRONMENTAL TECHNOLOGY

Ecological Engineering & Environmental Technology, 2025, 26(8), 363–374
https://doi.org/10.12912/27197050/208417
ISSN 2719–7050, License CC-BY 4.0

Received: 2025.06.19
Accepted: 2025.07.19
Published: 2025.08.01

Evaluating ecosystem recovery on degraded lands restoration using satellite-based spatial indicators in Mount Halimun Salak National Park, Indonesia

Theresa Vindri Pramesti[1*], Siti Badriyah Rushayati[2], Lilik Budi Prasetyo[2]

[1] Tropical Biodiversity Conservation Study Program, Faculty of Forestry and Environment, IPB University, Bogor, Indonesia
[2] Department of Forest Conservation and Ecotourism, Faculty of Forestry and Environment, IPB University, Bogor, Indonesia
* Corresponding author's e-mail: theresavindri@apps.ipb.ac.id

ABSTRACT

Ecosystem restoration efforts are undertaken in degraded forest areas impacted by anthropogenic disturbances, particularly agricultural expansion, to mitigate the effects of global warming. One of the primary challenges in implementing restoration programs is the difficulty in monitoring their effectiveness, primarily due to limited accessibility and the extensive spatial area of the restoration site. This limitation can be addressed by applying remote sensing technologies, which enable continuous, large-scale monitoring of landscape dynamics with high temporal and spatial efficiency. This study assesses the recovery of ecosystem services over 14 years in a restoration area within the corridor habitat of Gunung Halimun Salak National Park, Indonesia. The assessment focuses on three critical ecosystem service functions: microclimate regulation, biodiversity conservation, and carbon sequestration. Spatial analysis was conducted using Landsat satellite imagery to quantify changes in land surface temperature (LST), forest canopy density (FCD), and net primary productivity (NPP), in addition to assessing landscape structure through fragmentation metrics, including number of patches (NP), edge density (ED), mean shape index (MSI), and interspersion and juxtaposition index (IJI). The results indicate that while restoration efforts have facilitated partial recovery of ecosystem functions, the original ecological integrity of forest ecosystem services has not yet been fully restored. Nonetheless, integrating remote sensing data with landscape ecological indicators provides a practical and scalable method for assessing the dynamics of ecosystem service recovery in large and inaccessible restoration areas.

Keywords: corridors, ecosystem restoration, restoration, spatial analysis.

INTRODUCTION

Tropical deforestation and forest degradation have significantly reduced forest cover, with 17% of tropical moist forests lost since 1990 (Vancutsem et al., 2021). These changes have contributed substantially to increased atmospheric greenhouse gas concentrations (Harris et al., 2012) and biodiversity loss (Dubey et al., 2022). If current disturbance rates persist, intact tropical forests may disappear entirely in some regions by 2050, underscoring the urgent need for effective conservation policies (Vancutsem et al., 2021) and large-scale forest restoration (Pita et al., 2024). Forest restoration is crucial for mitigating climate change, conserving biodiversity, and maintaining ecosystem services (Aerts and Honnay, 2011). Although restoration initiatives have been implemented in many tropical countries, many have failed due to various challenges. Key factors contributing to these failures include insufficient consideration of genetic diversity and site suitability in selecting planting materials (Thomas et al., 2015), lack of local community engagement, and misalignment between restoration objectives and community needs (Höhl et al., 2020). Environmental disturbances, such as wildfires, also present significant barriers to success (Fawzi et al., 2020). Despite extensive reforestation efforts in Indonesia, the success of restoration remains low, with only 1% of replanted areas demonstrating successful ecological recovery (Fawzi et al., 2020). To enhance restoration outcomes, efforts must prioritize fire management, weed control, accurate cost estimations, and ecologically appropriate restoration strategies (Fawzi et al., 2020). Equally important is implementing long-term monitoring using efficient and advanced technologies, as conventional monitoring methods are often time-consuming and cost-prohibitive.

Remote sensing technologies offer a promising alternative for long-term monitoring, providing scalable and cost-effective tools to assess forest restoration progress across large spatial and temporal scales (de Almeida et al., 2020). This study aims to monitor ecosystem recovery and evaluate restoration outcomes in restoration areas and their adjacent landscapes within the Gunung Halimun Salak National Park (HSNP) corridor from 2011 to 2024, using a functional ecosystem approach focused on three key services: microclimate regulation, habitat and biodiversity conservation, and carbon productivity. Restoration is considered successful when these functions in the restoration area have values equivalent to those in the surrounding forest areas.

METHODS

Location

This study was conducted in the habitat corridor connecting Mount Salak and Mount Halimun within Gunung Halimun Salak National Park (GHSNP), the largest remaining expanse of upland and submontane tropical rainforest on Java, covering approximately 113,000 hectares (Figure 1). The corridor supports wildlife movement and high biodiversity, including endemic and endangered species such as the Javan gibbon, leopard, and hawk-eagle. Despite its protected status, the park continues to face ongoing threats from illegal land use, poaching, and degradation, underscoring the need for integrated conservation, restoration, and long-term monitoring. The study focuses on two blocks of restoration area – Gunung Kendeng (120 ha, planted in 2019) and Pasir Bendil (50 ha, planted in 2012) – along with the surrounding corridor area. Both blocks are located within the same village, with the same soil typesa – namely a complex of latosol and andosola – and at the same elevation (900–1200 m above sea level). Historically, both blocks were production forests managed by the state-owned company Perhutani before 2003, and were cultivated by local communities through an agroforestry (*tumpang sari*) scheme. This system allowed farmers holding cultivation rights to farm while also tending the trees that were planted.

Data collection and analysis

Data collection begins with downloading satellite imagery from the United States Geological Survey (USGS) via the EarthExplorer platform (earthexplorer.usgs.gov), including Landsat 7/enhanced thematic mapper (ETM) imageries for 2011 and 2012, and Landsat 8/operational land imager (OLI) imageries for 2013 to 2024. Before

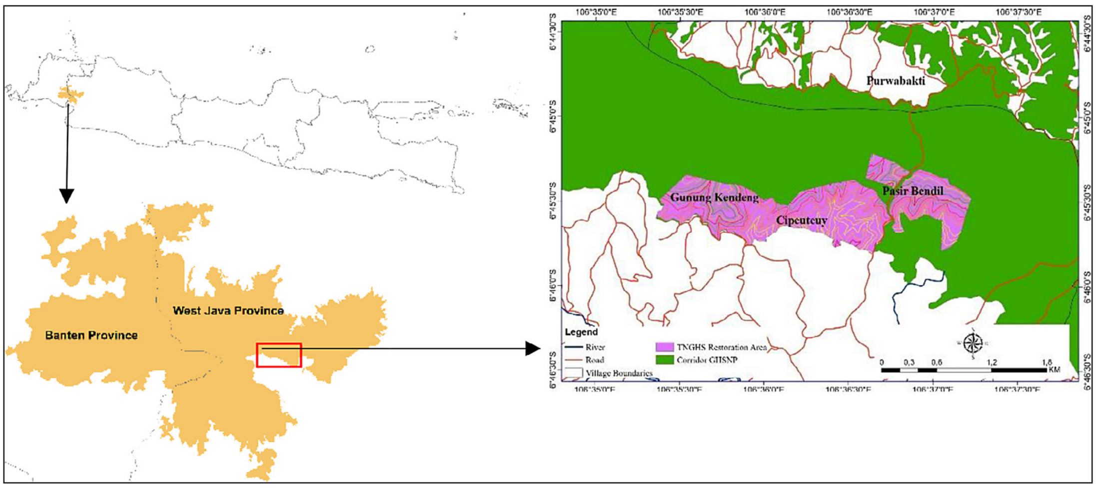

Figure 1. Study site – corridor of GHSNP

analysis, gaps in the SLC-off data from Landsat 7/ETM were filled using band-specific gap mask files using QGIS. Both Landsat datasets were used to calculate LST, NPP, and FCD. Meanwhile, Landsat 5/Thematic Mapper (TM) was used for land cover classification; however, the imagery was not downloaded, as it was processed directly using Google Earth Engine (GEE).

Land cover identification and accuracy assessment

For the land cover classification process, Landsat 5/TM satellite data were used for the years 2011 and 2012, and Landsat 8/OLI data were used for the years 2013 to 2024. The surface reflectance imagery was accessed and processed through Google Earth Engine (GEE) to generate annual cloud-free composites. Imagery for each year was filtered based on acquisition dates spanning from June 1 to September 30, corresponding to the dry season. It was limited to the spatial extent of the study area. This temporal filtering aimed to minimize cloud cover and improve image quality. A custom cloud masking function was applied using the pixel_qa band to mask out clouds, cloud shadows, and other low-quality pixels. The cloud-masked images were composited using the median pixel value to reduce the influence of residual clouds and outliers. The composite images were calibrated using the standard surface reflectance scaling factor (multiplying by 0.0001), then clipped to the study area *boundary*.

The images were then processed and analyzed for land cover classification using a supervised classification approach with the Random Forest algorithm in Google Earth Engine. Classification was performed using training samples obtained from high-resolution image interpretation, and the land cover types classified included forest, shrub, settlement, and agricultural.

To ensure the reliability of the classification results, an accuracy assessment was performed using overall accuracy and Kappa coefficient as evaluation metrics. For this purpose, the dataset was divided into 70% training data and 30% validation data. The Kappa coefficient is estimated based on the confusion matrix, which compares the agreement between the classified land cover labels and the independent ground-truth validation sample. This matrix measures the degree of agreement beyond chance by measuring the consistency between the predicted classes and the reference data. According to the threshold recommended by Viera and Garet (2005), the classification map is only used for further analysis if the overall accuracy and Kappa statistic achieve a minimum accuracy level of greater than 80%. The GEE script for the land cover classification and its accuracy assessment is presented in the supplementary document.

Climate amelioration

Microclimate improvement was assessed by measuring changes in land surface temperature (LST). The decreasing trend in LST indicates an improvement in microclimate conditions in the restored area, indicating the effectiveness of the restoration program. The procedure for calculating LST follows the method developed by the United States Geological Survey (USGS, 2016).

LST calculations are carried out using band six on Landsat 7/ETM and bands 10 and 11 on Landsat 8/OLI, which are thermal bands. However, for NDVI calculations, use bands 3 and 4 on Landsat 7/ETM and bands 4 and 5 on Landsat 8/OLI The LST calculation procedure with detailed steps is presented in Table 1.

Forest canopy density

The forest canopy density (FCD) model is a proxy for estimating forest canopy densitya – the proportion of land area covered by the vertical projection of tree canopies – which is widely used to indicate forest condition and degradation status. The FCD model integrates vegetation and bare soil indices obtained from multispectral satellite imagery, combining them through a fuzzy logic approach to estimate canopy density per pixel. In this study, FCD estimation follows the methodology published by Rikimaru (2002) (Table 2).

Net primary productivity

Net primary productivity (NPP) is a fundamental ecological metric that measures the rate at which plants produce biomass through photosynthesis after accounting for losses due to plant respiration. As such, NPP is a valuable indicator of restoration success, with higher NPP values reflecting healthier, more productive vegetation in restored areas. For the NPP analysis, Landsat 7/ETM satellite imagery was used for the years 2011 and 2012, and Landsat 8/OLI imagery for the years 2013 to 2024. Estimating NPP involves a series of processing steps, as outlined in Table 3.

Table 1. Land surface temperature (LST) data processing

Steps	Data processing	Equation	Description
1.	Radiometric correction to TOA reflectance	$L\lambda = \frac{(L_{max}-L_{min})}{(Qcal_{max}-Qcal_{min})}$ x (Q_{cal} - Q_{min}) + + L_{min} (Landsat 7) $L\lambda = MLQ_{cal} + AL$ (Landsat 8)	$L\lambda$ – radiance spectral *TOA* (W/m²·sr·μm), *ML* – radiance mult band, *AL* – radiance add band, Q_{cal} – digital number (DN) pixel value (e.g., 1–255)
2.	Temperature brightness	$T_b = \left(\frac{K_2}{ln\left(\frac{K_1}{L_\lambda}+1\right)}\right)$ -273,15	T_b – temperature brightness, K_1 – calibration constant 1, K_2 – calibration constant 2, • Band 6 of Landsat 7/ETM: K_1 = 666.09, K2 = 1282.71 • Band 10 of Landsat 8/OLI: K_1 = 774.8853, K2 = 1321.0789
3.	Normalized difference vegetation index	$NDVI = \frac{NIR-RED}{NIR+RED}$	*NIR* – near infrared radiation (band 5 of Landsat 8/OLI and band 4 of Landsat 7/ETM), *RED* – red band radiation from pixel (band 4 of Landsat 8/OLI and band 3 of Landsat 7/ETM)
4.	Proportion of vegetation	$Pv = \left(\frac{NDVI - NDVI_{min}}{NDVI_{max} - NDVI_{min}}\right)^2$	$NDVI_{min}$ – lowest value NDVI, $NDVI_{max}$ – highest value *NDVI*
5.	Land surface emissivity	$\varepsilon = m\,Pv + n$ $\varepsilon = 0.004\,Pv + 0.986$	ε – land surface emissivity, *Pv* – proportion of vegetation
6.	Land surface temperature	$LST = \frac{Tb}{\left[1 + \left(\frac{\lambda * Tb}{c2}\right) \times ln\,\varepsilon\right]}$	λ – wavelength of emitted radiance (10.895 μm), $c2 = h \times \frac{c}{s}$ = 14388 μmK

Table 2. Forest canopy density (FCD) data processing

Steps	Data analysis	Equation	Description
1.	Advanced vegetation index	$AVI = \sqrt[3]{(NIR) \times (1 - RED) \times (RED - NIR)}$	*NIR* – near infrared radiation (band 5 of Landsat 8/OLI and band 4 of Landsat 7/ETM), *RED* – red light radiation from pixel (band 4 Landsat 8 and band 3 Landsat 7/ETM)
2.	Bare soil index	$BI = \frac{(RED+SWIR) - (NIR+BLUE)}{(RED+SWIR) + (NIR+BLUE)}$	*SWIR* – shortwave infrared (band 6 of Landsat 8/OLI and band 5 of Landsat 7/ETM), *BLUE* – blue band radiation from pixel (band 2 of Landsat 8/OLI and band 1 of Landsat 7/ETM)
3.	Shadow index	$SI = \sqrt[3]{(1 - BLUE) \times (1 - GREEN)*(1 - RED)}$	*GREEN* – green band radiation from pixel (band 3 of Landsat 8/OLI and band 2 Landsat 7/ETM)
4.	Thermal index	$TI = K_2/Ln(\frac{K1}{L\lambda+1})$	*TI* – temperature brightness, K_1 – calibration constant 1, K_2 – calibration constant 2, $L\lambda$ – radiance spectral TOA
5.	Principal component analysis (PCA)	• a PCA was conducted between AVI and BI to obtain VD (Vegetation Density) • a PCA analysis between SI and TI to obtain SSI (Scaled Shadow Index)	PCA was performed using tools in QGIS
6.	Forest canopy density	$FCD = \sqrt{(VD \times SSI + 1)} - 1$	*FCD* – forest canopy density, *VD* – vegetation density, *SSI* – scaled shadow index.

Landscape metrics

Landscape metrics are spatial analysis tools used to quantify the structure, composition, and configuration of land cover patches in a landscape mosaic. These metrics provide valuable insights into landscape fragmentation, connectivity, and spatial heterogeneitya – key indicators in assessing ecosystem integrity, particularly in restoration monitoring. In this study, landscape metrics were computed using the landscape metrics package (Hesselbarth et al., 2019) in RStudio, based on classified land cover maps derived from Landsat satellite imagery. The land cover maps were first standardized by applying a 250 × 250 m spatial grid, and only patches larger than 1 pixel (≥ 250 m²) were included to minimize noise from minor artifacts and classification errors. The following class-level metrics were calculated:

- Number of patches (NP) – indicates the total number of discrete land cover patches for each class. A higher NP reflects increased fragmentation.

Table 3. Net productivity primer (NPP) data processing steps

Steps	Data analysis	Rumus
1.	NDVI (Myneni and Williams, 1994)	$NDVI = \frac{NIR-RED}{NIR+RED}$
2.	Fraction photosynthetically active radiation (Moran et al, 1995)	$FPAR = 1.24 \times NDVI - 0.168$
3.	Light use efficiency (Myneni and Williams, 1994)	LUE (gC/MJ) = $0.5 + (1.5 \times NDVI)$
4.	Albedo (Liang, 2001)	$\alpha\ L7 = (0.356 \times B1) + (0.13 \times B3) + (0.373 \times B4) + (0.085 \times B5) + (0.072 \times B7)$ $\alpha\ L8 = (0.356 \times B2) + (0.13 \times B4) + (0.373 \times B5) + (0.085 \times B6) + (0.072 \times B7) - 0.018$
5.	Total solar radiation (Liang, 2001)	$R_S\,(\mathrm{MJ/m^2}) = (1-\alpha) \times s \times 0.0864$
6.	Photosynthetically active radiation (Moran et al., 1995)	$PAR = f \times R_s$ f – fraction of photosynthetically active radiation (typically 0.5)
7.	Absorb photosynthetically active radiation (Gaffney et al., 2018)	$APAR = FPAR \times PAR$
8.	Gross primary productivity (Liu et al., 2021)	$GPP = APAR \times LUE$
9.	Net productivity primer (Zanotelli et al., 2013)	$NPP = GPP - R_a$ NPP (gC/m²/day) = $GPP - (0.5 \times GPP)$ NPP (ton C/ha/year) = NPP (gC/m²/day) × 10.0000 × 365 ÷ 1.000.000

- Mean shape index (MSI) – measures the average shape complexity of patches. MSI values close to 1 indicate regular (compact) shapes, while higher values suggest more irregular and fragmented patches.
- Edge density (ED) – represents the total length of edge per unit area (usually in meters per hectare, m/ha). ED captures the extent of edge effects, which are ecologically important in fragmented landscapes.
- Interspersion and juxtaposition index (IJI) – quantifies the degree to which different patch types are interspersed. IJI values range from 0 (clumped/segregated) to 100 (evenly interspersed), providing insight into landscape connectivity and mixing

These metrics were selected based on their relevance to forest fragmentation analysis and landscape ecological monitoring, as recommended by McGarigal and Marks (1995) and implemented by Hesselbarth et al. (2019). The calculations allow for tracking spatial changes in land use and land cover structure, especially concerning forest conservation and restoration programs within the study area.

RESULT AND DISCUSSION

Land cover changes

The natural forest areas within the Mount Halimun Salak National Park (TNGHS) have experienced a reduction in size due to logging activities and land-use conversion (Prasetyo et al., 2006). The remaining forest areas have been designated production forests, protected forests, and ecological corridors (GHSNP, 2008). In addition, there are plantation and agricultural areas within the corridor region (Sardjo et al., 2022). Over the past 14 years, the TNGHS corridor has undergone notable changes in land cover. These changes are illustrated in Figure 2. The forest area has increased due to restoration activities collaborating with the TNGHS authorities. Part of the TNGHS corridor was previously community-cultivated land when it was still classified as production forest managed by the state-owned company of Perhutani (Sardjo et al., 2022), resulting in agricultural areas. The increase in settlement area is due to the existence of enclaves. These settlements cannot be removed, as they have existed since before the Dutch colonial period (Dewi et al., 2023). The extent of shrub cover has fluctuated due to land cover changes around the corridor (Prasetyo and Setiawan, 2006).

Surface temperature changes

LST values have changed in magnitude over 14 years. Changes in LST in the corridor area and its surroundings are shown in Figure 3.

Areas with lower surface temperatures are predominantly forested, while other land cover types dominate areas with higher surface temperatures. In 2017, the blue areas – representing clouds with the lowest surface temperatures – obscured the

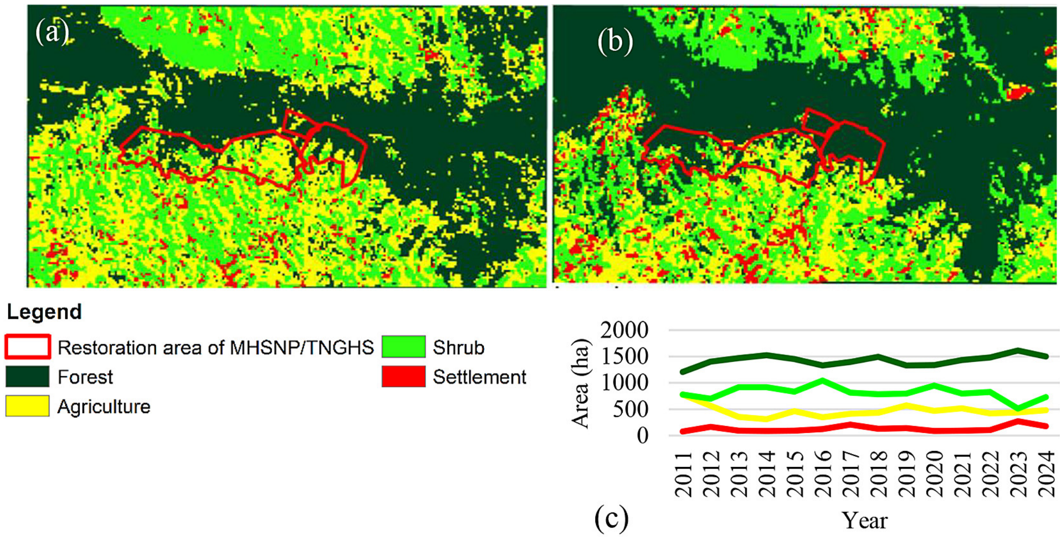

Figure 2. Land cover changes within 14 years after restoration, (a) 2011, (b) 2024, (c) trends of land cover changes 2011–2024

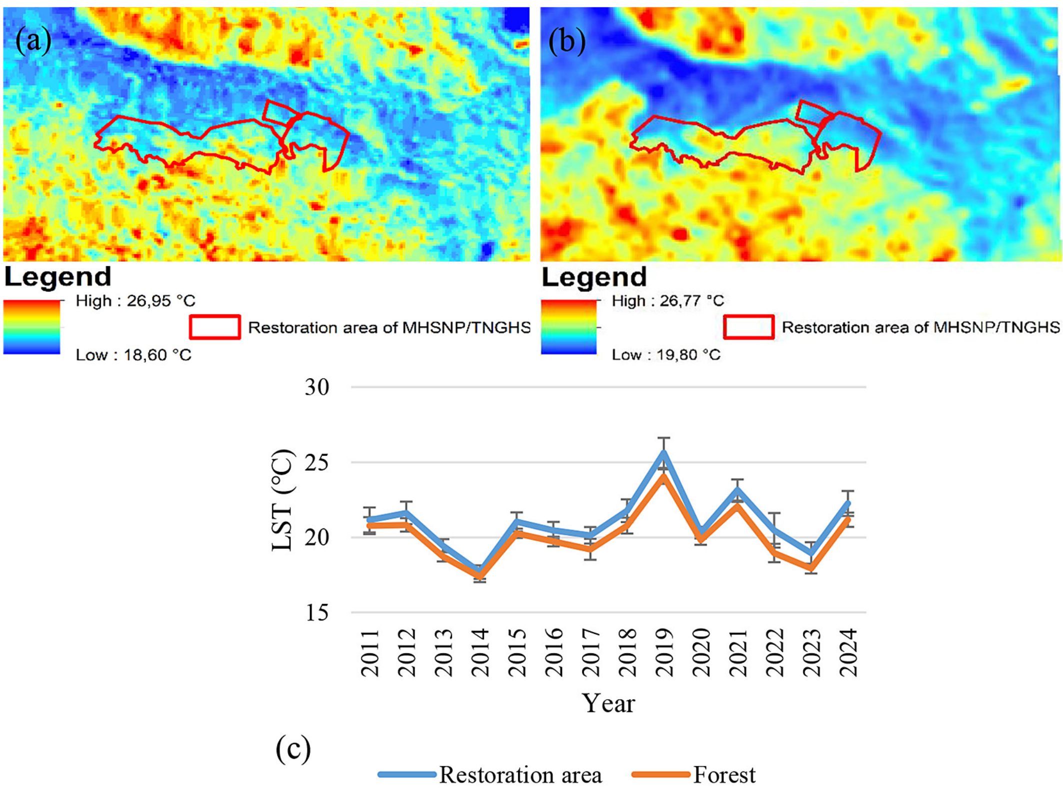

Figure 3. Land surface temperatures (LST) changes within 14 years after restoration, (a) 2011, (b) 2024, (c) trends of average LST 2011–2024

visibility of forest cover, which exhibits relatively low temperatures compared to other land covers, thus making it less distinguishable in the imagery. Guo-yu et al. (2013) explain that vegetated areas can lead to high levels of evapotranspiration, which increases air humidity and subsequently lowers temperature. Comparative analysis of LST between restoration and intact forest areas reveals that revegetated zones exhibit marginally higher mean LST values. These findings suggest that ecosystem restoration contributes to moderating surface temperature trends, although thermal conditions in restored areas have not yet equilibrated with those of mature forests.

Canopy density changes

Canopy density is the ratio between the canopy area and the land surface area. The higher the percentage value of canopy cover, the denser the vegetation (Hartoyo et al., 2021). The FCD value can describe the level of forest degradation and thus serve as a reference for restoration activities (Rikimaru et al., 2002). Figure 4 shows the dynamics of FCD changes.

At the initial stage of restoration, the FCD increased rapidly, followed by a period of stabilization and subsequent decline. This pattern likely reflects the dominance of fast-growing pioneer species that initially colonize the restored area. As these pioneer species are gradually replaced or outcompeted by slower-growing climax species, the overall FCD tends to decrease. Based on the observed trend in FCD dynamics, the canopy density in revegetated areas has not yet reached the levels characteristic of natural forest ecosystems. Nevertheless, the FCD has shown a marked increase compared to the early planting phase, indicating positive vegetation development. According to Suganuma and Durigan (2014), canopy cover is a reliable indicator for assessing the success of forest restoration.

Net primary productivity trend

Net primary productivity refers to the amount of net carbon absorbed by vegetation after subtracting the carbon used for activities such as respiration (Park et al., 2021). NPP can reflect the condition and changes in an ecosystem (Wei et al., 2018). The NPP results are shown in Figure 5.

Settlement areas do not absorb carbon, resulting in the lowest NPP values. Shrubland areas exhibit higher NPP than other land cover types (Li et al., 2023). Annual fluctuations in NPP occur due to variations in photosynthesis rates, which are influenced by sunlight exposure. In general, NPP values in revegetated areas remain lower than those in forested regions, indicating that ecosystem recovery in carbon absorption still requires considerable time.

Number of patch trend

The number of patch for forests indicates the quantity and composition of forest patches within the landscape, and it also indicates habitat fragmentation (Rutledge, 2003). The NP calculation results are shown in Figure 6. The number of forest patches (NP) across the entire

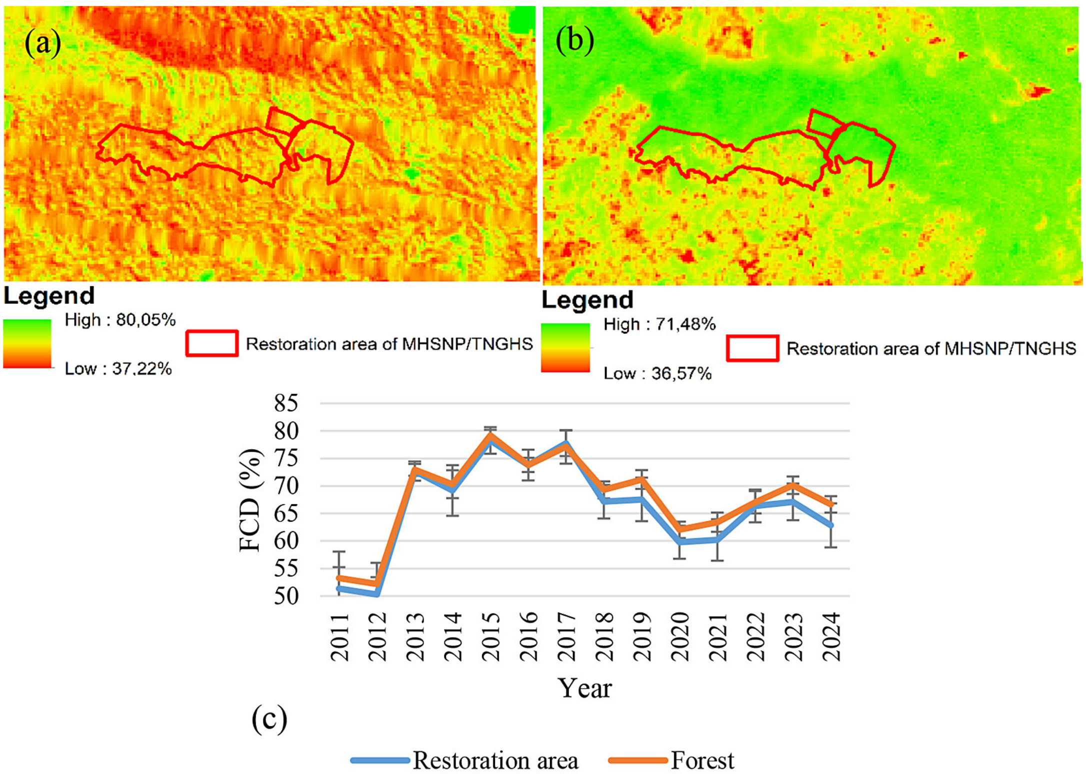

Figure 4. Forest canopy density (FCD) changes within 14 years after restoration, (a) 2011, (b) 2024, (c) trends of average FCD 2011–2024

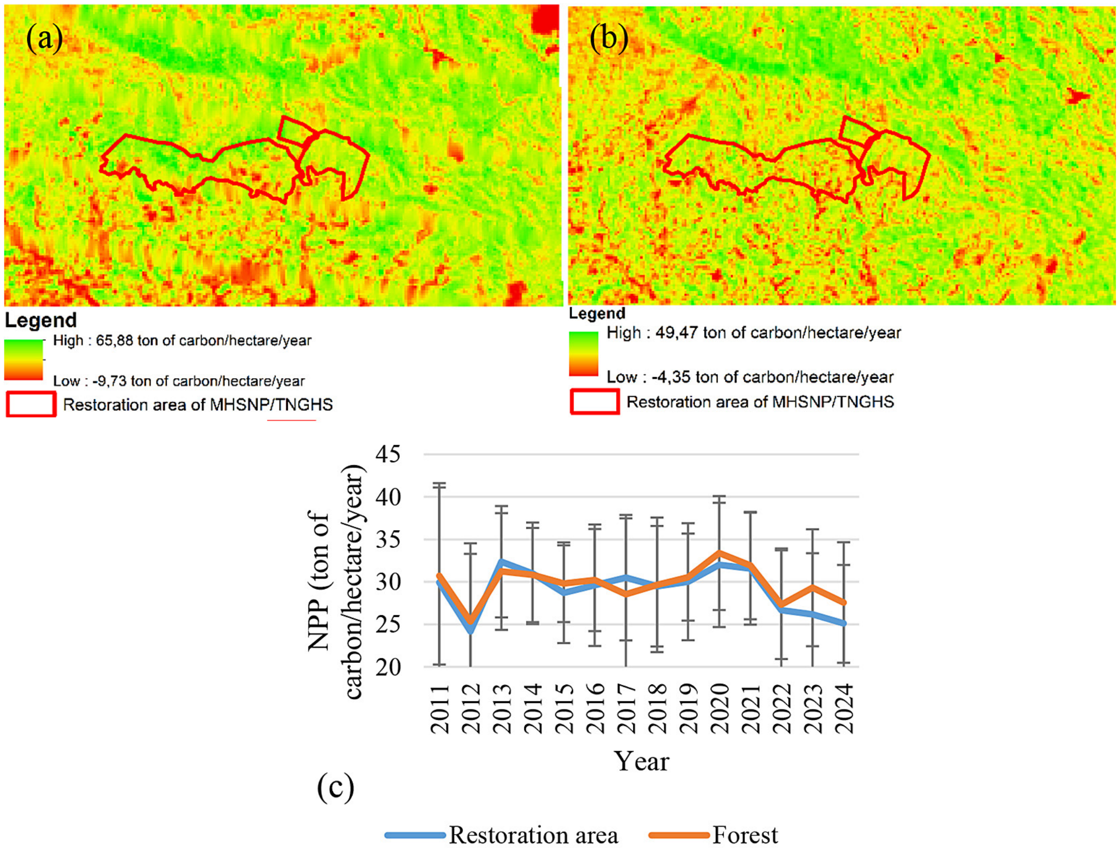

Figure 5. Net productivity primer (NPP) changes within 14 years after restoration, (a) 2011, (b) 2024, (c) trends of average NPP changes 2011–2024

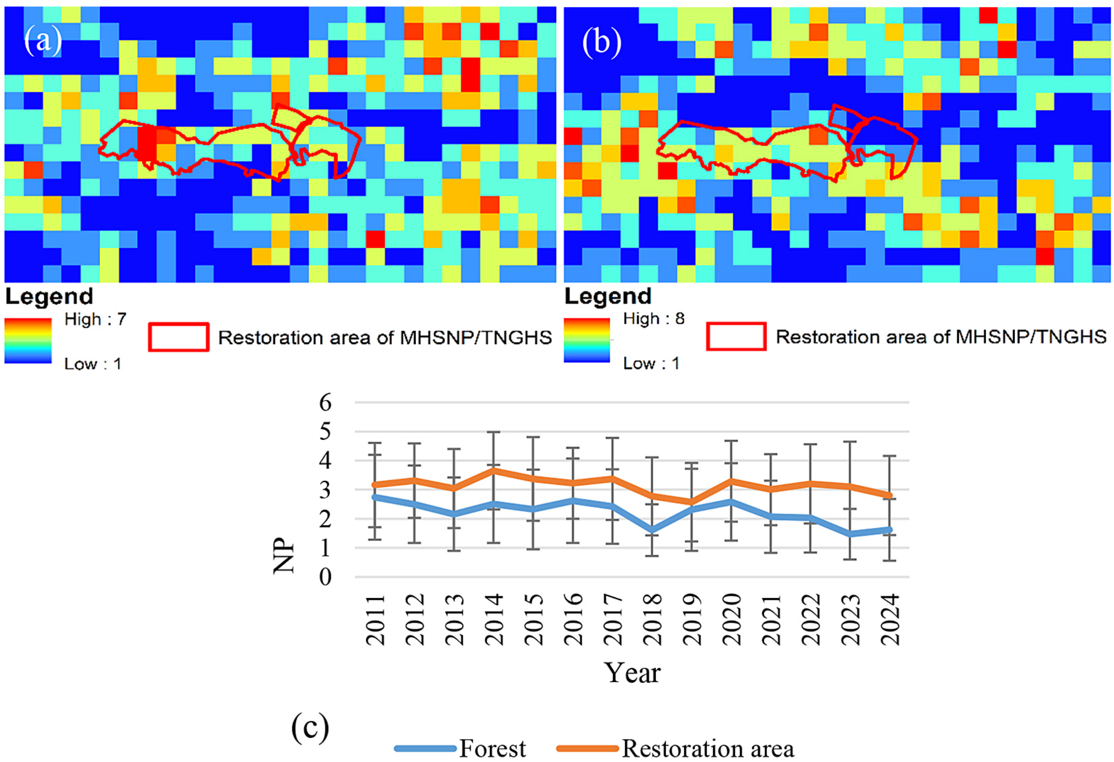

Figure 6. Number of patches (NP) within 14 years after restoration, (a) 2011, (b) 2024, (c) trends of average NP 2011–2024

study area fluctuated, but overall, no significant changes occurred. Similarly, in the regions revegetated, the forest NP remained relatively constant. This indicator suggests that there has not been a notable increase in forest patches within the revegetated areas.

Edge density trend

Edge density is the total length of landscape edges divided by the total landscape area (Sertel et al., 2018). ED is measured in meters per hectare (m/ha) (Flowers et al., 2020). The ED calculation results are shown in Figure 7.

Mean shape index trend

The mean shape index reflects the level of complexity in patch shapes, relative to the shape of a circle or square (McGarigal and Marks, 1995). MSI is calculated by dividing each patch's perimeter by the square root of its area (Flowers et al., 2020). The MSI calculation results are shown in Figure 8. MSI values approaching 1 indicate that patches have regular shapes, while higher values reflect increasing shape complexity and irregularity (McGarigal and Marks, 1995). Some forested areas show high MSI values despite having low fragmentation levels. The higher MSI values in revegetated areas than forested areas indicate that patches in revegetated land are more irregular and have a higher degree of fragmentation.

Interspersion and juxtaposition index trend

The interspersion and juxtaposition index describes the arrangement, relationships, and proximity of various habitats. A high IJI value indicates a high degree of dispersion and mixing of different land cover types (Masters et al., 2017). IJI strongly depends on the proximity of all patches to related edge areas (Turner et al., 1989). The IJI calculation results for the study site are shown in Figure 9.

IJI values approach 100 when all patch types are evenly adjacent, and decrease when this is not the case (Griffith et al., 2000). Low IJI values indicate low intermixing among patches in the landscape. Low IJI values in forest areas suggest that forests are not evenly distributed across the landscape. Coelho et al. (2022) state that non-forest classes tend to be

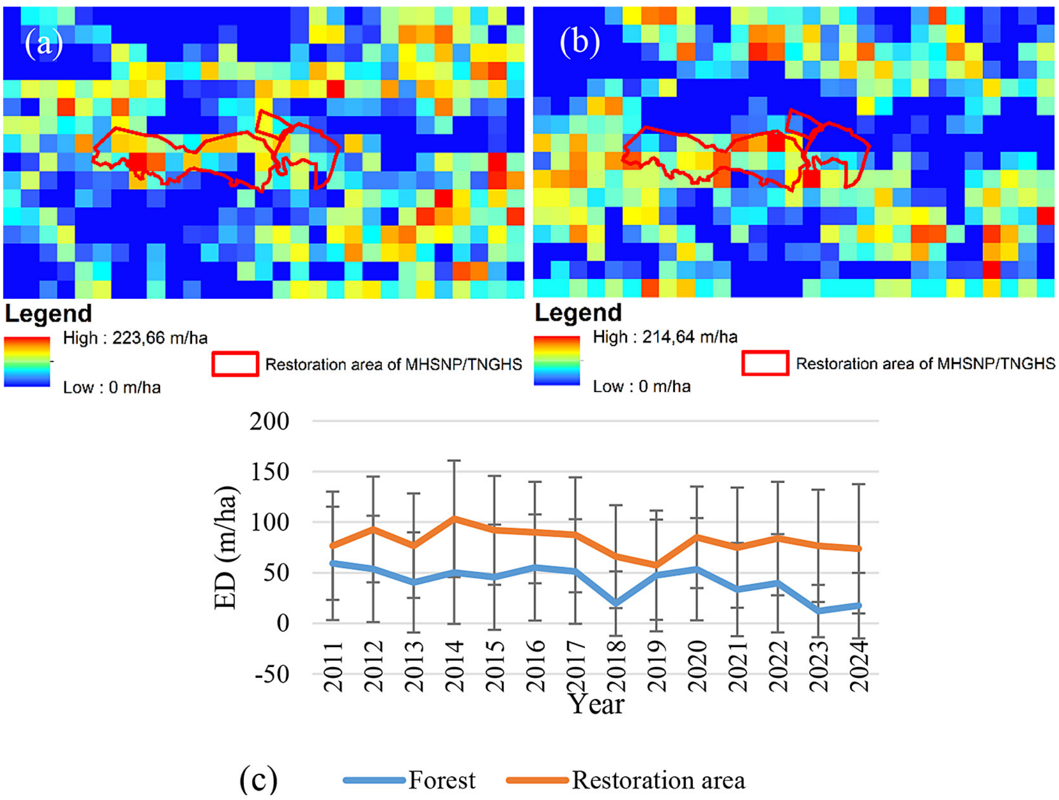

Figure 7. Edge density (ED) within 14 years after restoration, (a) 2011, (b) 2024, (c) trends of average ED 2011–2024

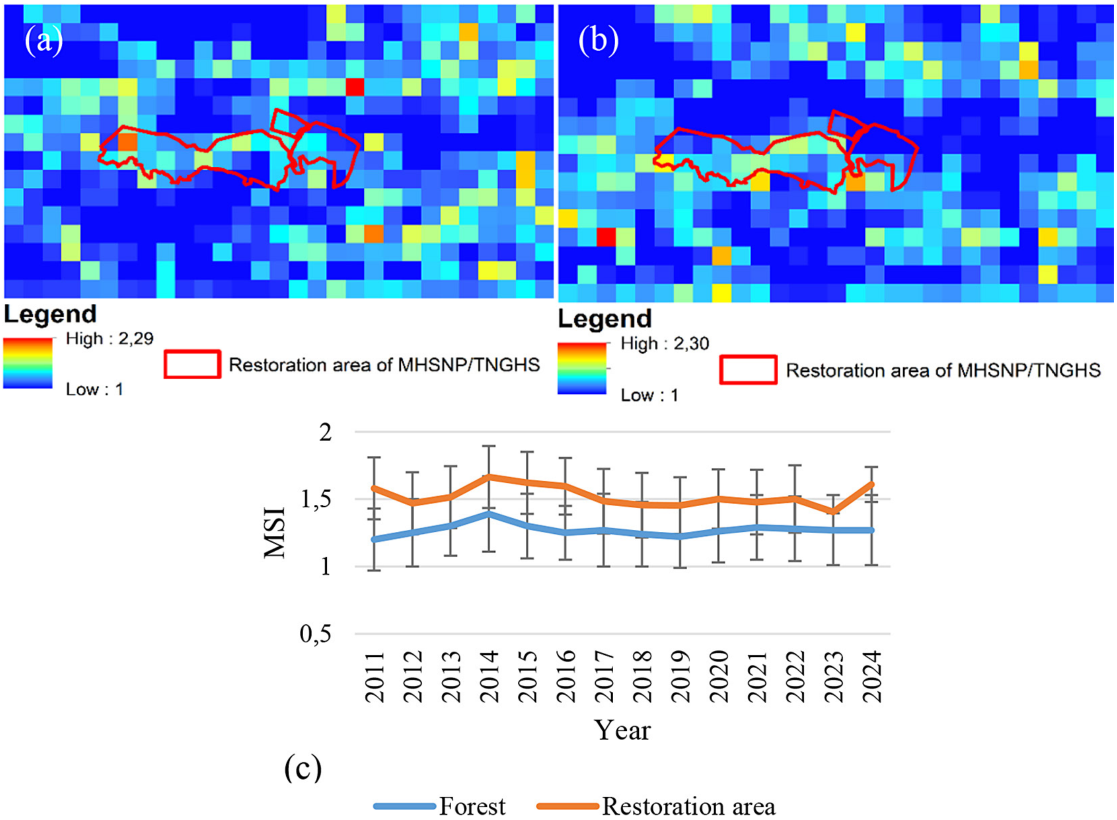

Figure 8. Mean shape index (MSI) changes within 14 years after restoration, (a) 2011, (b) 2024, (c) trends of average MSI changes 2011–2024

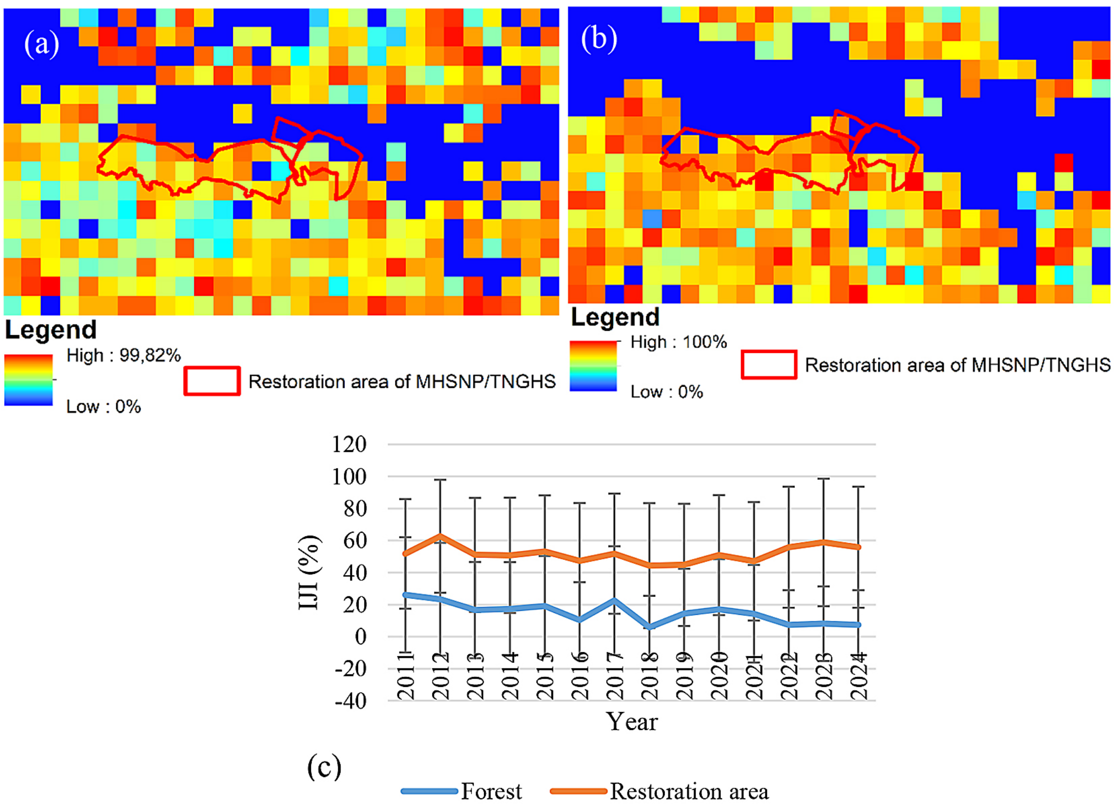

Figure 9. Interspersion and juxtaposition index (IJI) changes within 14 years after restoration, (a) 2011, (b) 2024, (c) trends of average IJI changes 2011–2024

more evenly dispersed than forest classes. This pattern is observed in the TNGHS corridor area and its surrounding areas.

CONCLUSIONS

The study proposed an approach that utilizes indices derived from satellite imagery to monitor the progress of restoration. Evaluation of ecosystem recovery in restoration lands within the TNGHS corridor, using satellite imagery data, indicates that these efforts have not yet restored the ecosystem functions of forested areas. This assessment is based on several indicators. LST values in revegetated areas nearly approach those of forests, and FCD values are moderate but not significantly different from those of forests, suggesting a potential to mitigate surface temperature increases and improve the microclimate. However, NPP values in revegetated lands remain below those of forest areas, indicating that restoration has not yet fully restored carbon productivity functions. Furthermore, fragmentation indices such as NP show stagnation in revegetated areas, while decreasing in forest areas. ED and MSI values are higher in restoration areas than in forests. Additionally, IJI values reveal that patches in revegetated areas are poorly dispersed. These factors suggest that restoration efforts have not been effective in reducing fragmentation. Therefore, it can be concluded that the ecosystem recovery process through restoration has not yet restored ecosystem functions to the level of natural forests.

Acknowledgements

The author would like to Environmental Analysis and Geospatial Modeling Laboratory for research funding and to all staff member for support this research.

REFERENCES

1. Aerts, R., Honnay, O. (2011). Forest restoration, biodiversity and ecosystem functioning. *BMC Ecology. 11*(29), 11–10. https://doi.org/10.1186/1472-6785-11-29
2. Coelho, A.M., Sousa, A.M.O., Goncalves, A.C. (2022). Spatial variability of forest species: case study for Alto Alentejo, Portugal. *Land. 12*(46), 1–15. https://doi.org/10.3390/land12010046
3. de Almeida, D.R.A., Stark, S.C., Valbuena, R., Broadbent, E.N., Silva, T.S.F., de Resende, A.F., Ferreira, M.P., Cardil, A. Silva, C.A., Amazonas, N. Zambrano, A.M.A., Brancalion, P.H.S. (2020). A new era in forest restoration monitoring. *Restoration Ecology. 28*(1), 8–11. https://doi.org/10.1111/rec.13067
4. Dewi, A.P., Peniwidiyanti, P., Hariri, M.R., Hutabarat, P.W.K., Martiansyah, I., Lailaty, I.Q., Munawir, A., Giri, M.S., Ambarita, E. 2021. Ethnobotany of food, medicinal, construction, and household utilities producing plants in Cikaniki, Gunung Halimun Salak National Park, Indonesia. *Journak of Mountain Science. 20*(1), 163–181. https://doi.org/10.1007/s11629-021-7108-5
5. Dubey, A., Mainani, R., Solanki, H. (2022). Biodiversity loss and its impacts on human well-being. *International Journal of Plant and Environment. 8*(3), 47–51. https://doi.org/10.18811/ijpen.v8i03.06
6. Fawzi, N.I., Helms, J., Emerson, A., Wibawanto, M.A. (2020). Forest restoration progress and lessons learned in Gunung Palung National Park, Indoneia. *Journal of Tropical Forest Science. 32*(2), 195–205. https://doi.org/10.26525/jtfs32.2.195
7. Flowers, B., Huang, K., Aldana, G.O. (2020). Analysis of the habitat fragmentation of ecosystems in Belize using landscape metrics. *Sustainability. 12*(7), 1–14. https://doi.org/10.3390/su12073024
8. Gaffney, R., Porensky, L.M., Gao, F., Irisarri, J.G., Durante, M., Derner, J.D., Augustine, D.J. (2018). Using APAR to predict aboveground plant productivity in semi-arid rangelands: spatial and temporal relationship differ. *Remote Sensing, 10,* 1–19. http://dx.doi.org/10.3390/rs10091474
9. GHSNP. (2008). Completion report of international internship on national park administration and management in West Java, Indonesia. GHSNP and Abogor Agricultural Institute.
10. Griffith, J.A, Martinko, E.A, Price, K.P. (2000). Landscape structure analysis of Kansas at three scales. *Landscape and Urban Planning. 52*, 45–61. https://doi.org/10.1016/S0169-2046(00)00112-2
11. Guo-yu, Q., Hong-yong, L., Qing-tao, Z., Wan, C., Xiao-jian, L., Xiang-ze, L. (2013). Effects of evapotranspiration on mitigation of urban temperature by vegetation and urban agriculture. *Journal of Integrative Agriculture. 12*(8), 1307–1315. https://doi.org/10.1016/S2095-3119(13)60543-2
12. Hartoyo, A.P.P., Sunkar, A., Ramadani, R., Faluthi, S., Hidayati, S. (2021). Normalized Difference Vegetation Index (NDVI) analysis for vegetation cover in Leuser ecosystem area, Sumatra, Indonesia. *Biodiversitas. 22*(3), 1160-1171. https://doi.org/10.13057/biodiv/d220311
13. Harris, N.L., Brown, S., Hagen, S.C., Saatchi, S.S., Petrova, S., Salas, W., Hansen, M.C.T., Potapov, P.V., Lotsch, A. (2012). Baseline map of carbon

emissions from deforestation in tropical regions. *Science. 336*, 1573–1576. https://doi.org/10.1126/science.1217962

1. Hesselbarth, M.H.K., Sciaini, M.,With, K.A., Wiegand, K., Nowosad, J. (2019). Landscapemetrics: an open-source r tool to calculate landscape metrics. *Ecography. 42*, 1648–1657. https://doi.org/10.1111/ecog.04617
2. Höhl, M., Ahimbisibwe, V., Stanturf, J.A., Elsasser, P., Kleine, M., Bolte, A. (2020). Forest landscape restoration-what generates failure and success? *Forests. 11*(938), 1–29. http://dx.doi.org/10.3390/f11090938
3. Li, T., Hu, J., Li, L., Liang, J., Li, D., Liu, Q. (2023). Temporal variation and factors influencing the stability of NPP in Chinese shrubland ecosystems. *Forests. 15*(531), 1–15. https://doi.org/10.3390/f15030531
4. Liang, S. (2001). Narrowband to broadband conversions of land surface albedo I Algorithms. *Remote Sensing of Environment. 76*, 213–238. https://doi.org/10.1016/S0034-4257(00)00205-4
5. Liu, X., Liu, Z., Liu, L., LU, X., Chen, J., Du, S., Zou, C. (2021). Modelling the influence of incident radiation on the SIF-based GPP estimation for maize. *Agricultural and Forest Meteorology. 307,* 1–12. https://doi.org/10.1016/j.agrformet.2021.108522
6. Masters, R., Ditchkoff, S., Farley, S.C. (2017). *Edge and other wildlife concepts*. Oklahoma State University.
7. McGarigal, K., Marks, B.J. (1995). *FRAGSTATS: Spatial pattern analysis program for quantifying landscape structure 51*. US Department of Agriculture, Forest Service, Pacific Northwest Research Station.
8. Moran, M.S., Maas, S.J., Pinter, P.J. (1995). Combining remote sensing and modeling for estimating surface evaporation and biomass production. *Remote Sensing Reviews. 12*(3–4), 335–353. https://doi.org/10.1080/02757259509532290
9. Myneni, R.B., Williams, D.L. (1994). On the relationship between FAPAR and NDVI. *Remote Sensing of Environment. 49*, 200–221. https://doi.org/10.1016/0034-4257(94)90016-7
10. Park, J.H., Gan, J., Park, C. (2021). Discrepancies between global forest net primary productivity estimates derived from MODIS and forest inventory data and underlying factors. *Remote Sensing. 13*(1441), 1–15. https://doi.org/10.3390/rs13081441
11. Pita, K., Wickham,S.B., Davis, E.L., Lauriault, P., Johnson, A., Le, N.Q., Mullally, S., Schang, K., Smitas-Kraas, M.M.A., Witmann, E., Trant, A.J. (2024). How does restoration ecology consider climate change uncertainties in forested ecosystems? *Restoration Ecology. 32*(8), 1–10. https://doi.org/10.1111/rec.14265
12. Prasetyo L.B., Setiawan, Y., Permadi, T. (2006). *Land use and land cover change Gunung Halimun Salak National Park 1989–2004*. JICA & Department of Forestry Indonesia.
13. Rikimaru, A., Roy, P.S., Miyatake, S. (2002). Tropical forest cover density mapping. *Tropical Ecology. 43*(1), 39–47.
14. Rutledge, D.T. (2003). *Landscape indices as measures of the effects of fragmentation: can pattern reflect process?* DOC Science Publishing.
15. Sardjo, S., Dharmawan, A.H., Darusman, D. Wahyuni, E.S. (2022) The agricultural expansion in conservation areas: the case of Gunung Halimun Salak National Park, West Java. *Forest and Society. 6*(2): 742–762. http://doi.org/10.24259/fs.v6i2.18380
16. Searchinger, T.D. (2010). Biofuels and the need for additional carbon. *Environmental Research Letters. 5,* 1–10. http://dx.doi.org/10.1088/1748-9326/5/2/024007
17. Sertel, E., Topaloğlu, R.H., Şalli, B., Yay, A.Y., Aksu, G.A. (2018). Comparison of landscape metrics for three different level land cover/land use maps. *International Journal of Geo-Information. 7*(10), 408–428. https://doi.org/10.3390/ijgi7100408
18. Suganuma, M.S. and Durigan, G. (2015). Indicators of restoration success in riparian tropical forests using multiple reference ecosystems. *Restor Ecol, 23*: 238–251. https://doi.org/10.1111/rec.12168
19. Thomas, E., Jalonen, R., Loo, J., Bozzano, M. (2015). Avoiding failure in forest restoration: the importance of genetically diverse and site-matched germplasm. *Unasylva. 245*(66), 29–36.
20. Turner, M.G. (1989). Landscape ecology: the effect of pattern on process. *Annual Review of Ecology and Systematics. 20*, 171–197. https://doi.org/10.1146/annurev.es.20.110189.001131
21. USGS. (2016). *Landsat 8 (L8) data users handbook*. U.S. Geological Survey.
22. Vancutsem, C., Achard, F., Pekel, J.F., Vieilledent, G., Carboni, S., Simonetti, D., Gallego, J., Aragão, L.E.O.C., Nasi, R. (2021). Long-term (1990-2019) monitoring of forest cover changes in the humid tropics. *Science Advances. 7*, 1–21. https://doi.org/10.1126/sciadv.abe1603
23. Viera, A.J., Garret. J.M. (2005). Understanding interobserver agreement: the kappa statistic. *Family Medicine. 37*(5), 360–363.
24. Wei, J., Chen, Y., Li, W., Zhu, C., Li, Z. (2018). Estimation of net primary productivity and its driving factors in the Ili River Valley, China. *Journal of Arid Land. 10*(5), 781–793. https://doi.org/10.1007/s40333-018-0022-1
25. Zanotelli D, Montagnani L, Manca G, Tagliavini M. (2013). Net primary productivity, allocation pattern and carbon use efficiency in an apple orchard assessed by integrating eddy covariance, biometric and continuous soil chamber measurements. *Biogeosciences. 10*, 3089–3108. https://doi.org/10.5194/bg-10-3089-2013